Crystallization of emulsified anhydrous milk fat: the role of confinement and of minor compounds. A DSC study

Mathilde Bayard[1, 2], Maud Cansell[1], Fernando Leal-Calderon[1,*]

[1] Université de Bordeaux, CNRS, Bordeaux INP, CBMN UMR 5248, 33600 Pessac, France

[2] Soredab, La Tremblaye, 78125 La Boissière Ecole, France

* To whom correspondence should be addressed: Fernando Leal-Calderon, CBMN, CNRS, UMR 5248, Université de Bordeaux, Bordeaux INP, Allée Geoffroy Saint Hilaire, 33600 Pessac, France
Tel: 33 (0)5 40 00 68 38
e-mail: fleal@enscbp.fr

Running title: Thermal behavior of emulsified anhydrous milk fat in presence of minor compounds

Key words: emulsions; anhydrous milk fat; crystallization; droplet size; minor compounds; supercooling.

Abbreviations: **AMF** Anhydrous Milk Fat; **DSC** Differential Scanning Calorimetry; **FA** Fatty Acid; **p-NMR** pulsed Nuclear Magnetic Resonance; **SC** Sodium Caseinate; **SDS** Sodium Dodecyl Sulfate; **SFC** solid fat content; **TAG** TriAcylGlycerol; **XRD** X-ray diffraction; **3:0** propionic acid; **18:1** oleic acid; **16:0** palmitic acid; **PPP** tripalmitin

Abstract

We examined the crystallization and melting of anhydrous milk fat (AMF)-in-water emulsions stabilized by sodium caseinate. Various additives at low concentrations (< 5 wt%), differing in their hydrocarbon chain length (propionic *vs.* palmitic acid), unsaturation (palmitic *vs.* oleic acid), and esterification state (palmitic acid *vs.* tripalmitin) were used to modulate AMF crystallization kinetics. Three emulsions with different average droplet diameters were cooled down from 60 °C to 4 °C. Fat crystallization was followed by DSC under dynamic (cooling) and static (isothermal) conditions. Propionic acid did not have any noticeable effect. Oleic acid favored supercooling and the formation of unstable polymorphs at short times but its impact faded after 48 h of isothermal storage. The impact of palmitic acid was related to its amphiphilic properties and vanished after 48 h. Tripalmitin influenced crystallization *via* volume effects that were persistent. It formed mixed crystals which extended the melting range of AMF.

1. Introduction

Numerous food products are based on oil-in-water emulsions (O/W) (salad sauces, milk...) or water-in-oil-emulsions (W/O) (butter, margarines…). In all cases, two immiscible fluids are involved, leading to metastable systems. Once fabricated, emulsions evolve towards the total phase separation of the two fluids under the effect of coalescence and Ostwald ripening, over time scales that may vary from hours to years (Bibette, Leal-Calderon, Schmitt, & Poulin, 2002). The kinetic stability and shelf life of emulsions is determined by the nature and concentration of the surface-active species (amphiphilic polymers, proteins, low molecular weight surfactants) that are adsorbed at the oil-water interface. It is well known that the presence of crystals in the dispersed phase of O/W emulsions may have profound consequences for their stability because of specific instabilities caused by protruding crystals (Fredrick, Walstra, & Dewettinck, 2010). Also, crystallization impacts the rheological properties. When fat droplets are attached to a gel protein network formed in the continuous phase, they act as active fillers and droplets crystallization may strongly enhance the gel firmness (Dickinson, 2012).

Milk fat is of special relevance in dairy products and this is why there is abundant literature about its crystallization, both in bulk phase and in the emulsified state. Crystallization of triacylglycerols (TAGs) is a two-stage process involving nucleation and growth (Metin & Hartel, 2005). The presence of impurities like dust particles which are almost inevitable in natural fats, or the contact with solid substrates (scraped surface of a heat exchanger, for example) during fat processing may favor a heterogeneous nucleation mechanism by catalyzing the formation of the first fat nuclei. Emulsification of anhydrous milk fat (AMF) in an aqueous phase leads to a divided state of the fat, its confinement in drops, more or less pronounced depending on their average size, and the

65 existence of a water/oil interface, covered by amphiphilic species. All these parameters
66 can modify the fat crystallization scenario in terms of nucleation, growth, polymorphism
67 and/or microstructure (Lopez, Lavigne, Lesieur, Keller, & Ollivon, 2001a; McClements,
68 2012). The impurities initially present in bulk fat become distributed within drops in the
69 emulsified state. The smaller the average droplet size, the greater the number of drops
70 and the smaller their volume. As a result, the probability of finding impurities likely to
71 induce heterogeneous nucleation in a drop decreases and it is generally accepted that
72 nucleation tends towards the homogeneous mode (McClements, 2012). This is why, in
73 order to induce crystallization, it is necessary to impose a higher degree of supercooling
74 as the average droplet size decreases (Walstra, Wouters, & Geurts, 2006; Lopez,
75 Lesieur, Bourgaux, Keller, & Ollivon, 2001b). Lopez et al. (2002) combined optical
76 microscope observations between crossed analyzers and Differential Scanning
77 Calorimetry (DSC) measurements coupled with X-ray diffraction (XRD) to study AMF
78 crystallization in emulsified systems. They demonstrated that the average drop diameter
79 affects the crystal size and/or the structure of the crystal network because of defects in
80 the organization of TAG molecules in the crystals, either directly due to the curvature of
81 the oil/water interface from which crystals are supposed to grow, or indirectly due to the
82 faster relaxation that can induce the formation of crystals of smaller size. Moreover, a
83 higher disorder and/or a smaller size of TAG crystals within the emulsion droplets was
84 observed, due to the faster supercooling relaxation induced by the decrease of droplet
85 size.

86 Milk fat crystals can exist at the nanoscale in different crystalline forms, called
87 polymorphs. The 3 main polymorphic forms encountered in TAGs are the α-hexagonal
88 form, the β' orthorhombic form, and the β triclinic form. They correspond to the lateral
89 arrangement and degree of tilt of fatty acid (FA) chains in space (Sato, 1999). A fourth

90 unstable polymorph, called sub-α, can be observed in AMF at very low temperatures (<-
91 8 °C) for rapid cooling rates (>|2.5 °C/min|) (ten Grotenhuis, van Aken, van Malssen, &
92 Schenk, 1999). In milk fat, different TAGs often associate and crystallize together to form
93 mixed crystals (Martini, Herrera, & Hartel, 2002). The α polymorph is likely to provide this
94 type of crystals since it is loose enough to incorporate TAGs of different FA compositions.
95 The β' form also allows such compositional versatility (Walstra et al., 2006). TAGs also
96 self-organize themselves in a so-called longitudinal arrangement. They form stacks,
97 generally over two (2L), three (3L) or six chain lengths (6L), depending on the nature of
98 FAs that compose them (Sato and Ueno, 2011).

99 Although the structure of AMF is largely dictated by its TAG composition and the
100 thermal history, minor exogenous compounds or compounds formed during dairy
101 processes can also influence the crystallization scenario and the physical characteristics
102 of the fat (Smith, Bhaggan, Talbot, & Malssen, 2011; Talbot, Smith, & Bhaggan, 2012;
103 Rønholt, Mortensen, & Knudsen, 2013; Sato, Bayés-García, Calvet, Cuevas-Diarte, &
104 Ueno, 2013; Bayés-García et al., 2015; Patel & Dewettinck, 2015; Bayard, Leal-Calderon,
105 & Cansell, 2017). Minor compounds can accelerate or inhibit both nucleation and
106 crystalline growth (Metin & Hartel, 2005; Smith et al., 2011; Rønholt et al., 2013; Sato et
107 al., 2013; Bayés-García et al, 2015; Bayard et al., 2017), and their influence can be
108 antagonistic, accelerating one while slowing the other (Talbot et al., 2012). In addition,
109 minor compounds can influence the polymorphic behavior, in particular by inhibiting some
110 phase transitions. They could also block growth sites during recrystallization in
111 polymorphic phase transitions involving crystal melting (Smith et al., 2011; Talbot et al.,
112 2012). Various factors determine the impact of modulators on crystallization and on the
113 resulting physical properties of AMF like their chemical nature (Wright & Marangoni,
114 2003; Smith et al., 2011), their concentration (Vanhoutte, Dewettinck, Foubert,

115 Vanlerberghe, & Huyghebaert, 2002; Foubert, Vanhoutte, & Dewettinck, 2004, Bayard et
116 al., 2017), and the processing conditions (Sato et al., 2013; Kaufmann, Kirkensgaard,
117 Andersen, & Wiking, 2013). It is worth noticing that most studies related to the impact of
118 minor compounds in AMF have been carried out in bulk systems.

119 In this paper, we examine AMF crystallization under confined conditions, *i.e.*, in
120 emulsion droplets, in the absence and in the presence of modulators at a concentration
121 less than or equal to 5 wt%. At such low concentrations, the presence of minor
122 compounds is not expected to modify the nanostructure of AMF crystals (Bayard,
123 Kaufmann, Leal-Calderon, & Cansell, 2021). However, depending on the nature of their
124 hydrocarbon chains, modulators can be water-soluble, can self-crystallize or may exhibit
125 surface-active properties and their impact on AMF crystallization can combine volume
126 and/or interfacial effects that have not been addressed so far. To illustrate this diversity,
127 3 FAs, namely propionic, palmitic and oleic acids, and a TAG, tripalmitin, were selected.
128 In a previous study devoted to bulk AMF crystallization, it was demonstrated that
129 propionic and oleic acids behaved as inhibitors, whilst palmitic acid and tripalmitin were
130 crystallization promotors (Bayard et al., 2017). The question arises as to whether these
131 properties are retained in the emulsified state. The average droplet size of the emulsions
132 was tuned by varying the emulsification conditions so that 3 mean diameters were
133 obtained. Fast cooling induced the formation of fat crystals whose kinetic evolution was
134 followed under isothermal and non-isothermal conditions. The crystallization state of AMF
135 was assessed by DSC during a fast-cooling step from 60 °C to 4 °C and after a storage
136 period of 90 min and 48 h under isothermal conditions, at 4 °C. Crystallization was also
137 visualized *in situ* using the pending drop method. Overall, our approach aims at providing
138 insight into the effect of average droplet size of the emulsion and of the chemical nature

139 of minor compounds on supercooling phenomena and on the crystallization scenario
140 during isothermal storage.
141
142 **2. Materials and Methods**
143
144 *2.1. Materials*
145 AMF was supplied by Corman SA (Goé, Belgium) and was used without further
146 purification. AMF was composed of approximately 6% short chain FAs (strictly less than
147 8 carbons), 20% midsize chains (with more than half of myristic acid), and 72% long
148 chains mainly represented by oleic acid (20 wt%), palmitic acid (32 wt%), and stearic acid
149 (9 wt%). Unsaturated chains represented 27% of the total FAs, oleic acid being the most
150 abundant one. The melting domain of AMF ranged from -40 °C to +37 °C. A low melting
151 AMF fraction (full melting for T> 10 °C; chain composition: C4-C6=7 wt%; C8 to C14= 19
152 wt%; C16= 23 wt%, C18:1= 32 wt%, C18= 7 wt%) of AMF provided by Corman (Goé,
153 Belgium) was used for surface tension measurements. Sodium caseinate (SC) with a
154 minimal protein content of 88% and a maximum moisture content of 6% was purchased
155 from Armor Protéines (France). All chemicals adopted as crystallization modulators were
156 from Sigma-Aldrich (Saint-Quentin Fallavier, France): palmitic acid (16:0, purity> 98%, M
157 = 256 g/mol), propionic acid (3:0, purity > 99.5%, M = 74 g/mol), oleic acid (18:1,
158 purity >95%, M = 282 g/mol) and tripalmitin (PPP, purity >85%, 100% triglyceride and
159 palmitic content >90%, M = 807 g/mol). Sodium Dodecyl Sulfate (SDS) was used to dilute
160 emulsions before droplet size measurements and sodium hydroxide was used to adjust
161 the pH.
162
163 2.2. *Emulsion fabrication*

164 The effect of modulators on AMF crystallization was studied on 3 emulsions of
165 different diameters. The concentration of the modulators with respect to AMF mass varied
166 between 0.5 and 5 wt%. Blends of AMF and crystallization modulators were first heated
167 at 85 °C to obtain a homogeneous melt. This procedure that consists in heating the fat at
168 least 10 °C above the temperature of the species with the higher melting point (16:0,
169 63 °C) is usually considered as sufficient to erase any crystal memory.
170 The emulsions formulated in this study were of the O/W type and were stabilized
171 by SC. The fat phase, either neat AMF or AMF+modulator, was the dispersed phase (40
172 wt%) and the continuous phase (60 wt%) was an aqueous solution at 3.33 wt% SC (2
173 wt% SC with respect to the whole emulsion mass). The aqueous and fat phases were
174 mixed in an IKA LR 1000 laboratory reactor (Germany) equipped with an Ultra-Turrax®
175 turbulent mixer with a S25-KV-25F rotor-stator dispersing unit, thermostatically controlled
176 at 60 °C. This setup prevented crystallization during shearing and provided agitation to
177 the system. The mixture to be emulsified (1.2 L) was subjected to an intense shear at
178 25,000 rpm for 10 min. The obtained emulsion was then stored at 60 °C for a period no
179 longer than 2h. From this primary emulsion, 2 daughter emulsions with reduced droplet
180 size were obtained using a Niro Soavi Panda, GEA (Italy) high pressure homogenizer at
181 two homogenizing pressures, 50 and 500 bars. The obtained emulsions were stored at
182 60 °C, between 1 and 8h, until use. Emulsions resulting from the 3 homogenization levels
183 (0, 50 and 500 bars) will be referred to as LD (“Large Diameter”), MD (“Medium Diameter”)
184 and SD (“Small Diameter”).
185 A specific protocol was adopted for the emulsion containing 3:0. Due to their high
186 polarity, short-chain FAs exhibit high water solubility (>3 mol/L) (Bell, 1973). Solubilization
187 of 3:0 in water led to a decrease in pH that reached the isoelectric point of SC (close to
188 4.8) and caused protein precipitation, which precluded emulsification. Thus, the pH of the

189 aqueous phase was adjusted by adding sodium hydroxide, prior to the emulsification. The
190 concentration of sodium hydroxide in the aqueous phase was fixed at 0.042 mol/L. After
191 emulsification, the final pH of the aqueous phase was equal to 6.3, close to that measured
192 for emulsions based on neat AMF (6.7 ± 0.1), and on AMF mixed with modulators with
193 very low water solubility: AMF+16:0 at 2.5 wt% (6.6 ± 0.1), and AMF+18:1 at 2.5 wt% (6.5
194 ± 0.1). Concentrations of 3:0 above 0.5 wt% were not probed as they required larger
195 amounts of sodium hydroxide likely to induce fast triglyceride hydrolysis because of the
196 initial basic pH conditions and to substantially increase the ionic strength in the aqueous
197 phase.
198
199 2.3. *Emulsion characterization*
200 Emulsions were imaged with a phase contrast microscope (BX53F, Olympus,
201 Japan). To facilitate the observation, they were diluted with a SDS aqueous solution at
202 8.10^{-3} mol/L. This surfactant is known to dissociate droplets potentially aggregated *via*
203 protein bridging, which enables the observation of single droplets (Demetriades &
204 McClements, 2000). Images were acquired using a 10.6-megapixel digital camera
205 (SC100, Olympus, Japan).
206 The size distributions were measured using a Mastersizer 3000 apparatus
207 (Malvern Instruments, UK). Static light-scattering data were transformed into size
208 distribution using Mie Theory. The droplet refractive index was 1.46 and that of the
209 aqueous phase was 1.33. The emulsions were submitted to a 100-fold dilution with an
210 aqueous phase at 8.10^{-3} mol/L SDS in order to disaggregate droplets. A small volume of
211 sample was then introduced under stirring at 1,200 rpm in the dispersion unit. Each
212 measurement was performed in triplicate. The droplet distributions were described in

terms of their volume-averaged diameter, D_v, surface-averaged diameter, D_s, and polydispersity, P, defined as:

$$D_v = \frac{\sum N_i D_i^4}{\sum N_i D_i^3}; \qquad D_s = \frac{\sum N_i D_i^3}{\sum N_i D_i^2}; \qquad P = \frac{1}{\overline{D}} \frac{\sum N_i D_i^3 (\overline{D} - D_i)}{\sum N_i D_i^3} \qquad \text{Equation (1)}$$

where $\overline{D}$ is the median diameter, *i.e.* the value for which the cumulative undersized volume fraction is equal to 50%, and N_i is the total number of particles with diameter D_i.

2.4. Differential scanning calorimetry

Thermal analyses were conducted on a differential scanning calorimeter (DSC 8500, Perkin Elmer, UK) in aluminum pans of 10 µL hermetically sealed. An empty, hermetically sealed aluminum pan was used as reference. Calibration was made with indium (melting point = 156.6 °C, melting enthalpy = ΔH_m = 28.45 J/g), and cyclohexane (melting point = 6.47 °C, ΔH_m = 31.8 J/g) at scanning rates of ± 5 °C/min. All DSC experiments were carried out in the temperature range from 4 °C to 60 °C. The heat flow was expressed in W/g of fat. For the sake of comparison, several plots were superimposed in the same graph. To facilitate the readability, the graphs were shifted vertically. The baseline corresponding to a zero-heat flow is given by the enthalpic signal between 40 and 50 °C.

The melting or crystallization enthalpy variation, ΔH, was determined from the total area of the thermographs between 4 °C and T_{offset}, the temperature at which the DSC signal reached the baseline in melting experiments, or T_{onset}, the initial crystallization temperature in cooling experiments (non-isothermal crystallization). When thermograms presented several endothermic or exothermic events, the characteristic temperatures were taken at the maximum of the peaks.

236 DSC thermograms were measured in triplicate for all crystallization experiments
237 and for melting experiments performed with emulsions containing neat AMF. A single
238 melting experiment was carried out for emulsions containing a modulator. In this case, for
239 the statical analysis, we adopted the same relative standard deviation (SD/mean) as that
240 of the emulsion based on neat AMF with comparable droplet size.
241
242 *2.5. Thermal programs*
243 The following operating conditions allowed to assess the evolution of fat
244 crystallization under dynamic (cooling) and static (isothermal) conditions (Figure SI1,
245 supplementary information):
246 - Controlled cooling ramp from 60 °C to 4 °C at -5 °C/min followed by an isothermal stage
247 at 4 °C for 90 min and by a melting ramp at +5 °C/min with continuous recording of the
248 heat flow by DSC.
249 - Quench at 4 °C, followed by storage for 48 h at 4 °C. Samples introduced in sealed
250 aluminum pans of 10 µL were warmed at 60 °C and were then located in a
251 thermostatically controlled chamber at 4 °C for 48 h. After that delay, the thermal
252 properties of the crystallized state were characterized by DSC following a melting ramp
253 at +5 °C/min.
254
255 *2.6. Surface tension measurements*
256 Surface tension measurements at the oil/water interface were performed at 25 °C
257 using the rising drop method (Tracker" apparatus from Teclis Instruments, France). Single
258 fat droplets of 5 µL were formed at the tip of a steel needle and images were recorded at
259 regular time intervals with a digital camera. A low melting AMF fraction that was fully
260 molten at the operating temperature was adopted for the measurements. The aqueous

phase contained SC at 0.33 wt%. The drop shape was fitted considering the Young-Laplace equation, the surface tension, γ, being the unique free parameter. The same setup was used to visually follow AMF crystallization. In this case, a larger AMF drop of 15 µL was formed at the tip of the needle to facilitate the observation and the concentration of the modulators 16:0 and PPP was 0.25 wt%.

2.7. Statistical analysis

Droplet diameters, onset, offset and peak temperatures, melting and crystallization enthalpies from DSC curves were expressed as mean values with standard deviation (mean ± SD). Comparisons were analyzed using a one-way analysis of variance followed by a pairwise t-test using R version 3.1.2. Differences with P-values <0.05 were considered to be statistically significant.

3. Results and discussion

We aim at assessing the influence on AMF crystallization of the droplet size and of the nature of the modulators. Interestingly, the additives under study cover different situations regarding their localization, either at the oil/water interface or in the droplets' core, which will allow a modulation of AMF crystallization based on bulk or interfacial effects. Both 18:1 and 16:0 FAs are surface-active and mainly oil-soluble (water solubility $<10^{-6}$ mol/L (Bell, 1973)); 3:0 and PPP are not expected to have any interfacial activity. As noted in Section 2.2, 3:0 is highly soluble in water and is distributed between the oil and aqueous phase. Being nearly insoluble in water, PPP is primarily present in the fat globules.

3.1 Main characteristics of the emulsions

286 Emulsions were characterized by droplet sizing based on light-scattering. The
287 main characteristics are provided in Table 1. The size distributions can be found in Figure
288 SI2 of supplementary information. Irrespective of the formulation, the 3 levels of
289 homogenization applied (0 bar, 50 bars, 500 bars) allowed to obtain emulsions whose
290 droplets had significantly different diameters but all exhibiting a roughly monomodal
291 distribution. The non-homogenized LD emulsion based on neat AMF had a volume-
292 averaged diameter, D_v of 6.0 μm, close to the average diameter in raw milk (Michalski,
293 Ollivon, Briard, Leconte, & Lopez, 2004). The homogenization at 50 bars (MD emulsion)
294 led to an average diameter of 2.2 μm. Homogenization at 500 bars (SD emulsion) resulted
295 in a submicron-sized emulsion of 0.8 μm (LD emulsion). Observations under the
296 microscope (Figure SI2-A in supplementary information) were consistent with the results
297 obtained *via* droplet sizing. The size distributions and average diameters obtained in the
298 presence of the modulators are almost identical to those reported for neat AMF except
299 for the LD emulsions containing 18:1 and 16:0 that have slightly smaller diameters
300 compared to neat AMF (Table 1). This can be interpreted as being due to the surface-
301 activity of both 18:1 and 16:0. Interfacial tension measurements were carried out using
302 the rising drop method. The concentration of SC in the aqueous phase was set at 0.33
303 wt% to avoid drop detachment due to excessively low interfacial tension (<4 mN/m). To
304 avoid the formation of fat crystals likely to perturb measurements, neat AMF was replaced
305 by a low melting AMF fraction. Studies on competitive adsorption in model emulsion
306 systems stabilized by pure milk proteins have shown that the presence of oil-soluble or
307 water-soluble surfactants during emulsification leads to a reduction in surface tension, in
308 the protein surface coverage and in the average droplet size of the resulting emulsions,
309 irrespective of the oil and of the protein nature (De Feijter, Benjamins, & Tamboer,
310 1987).The values obtained 1 h after forming the drop were 10.8 ± 0.5 mN/m, 6.2 ± 0.5

311 mN/m and 8.2 ± 0.5 mN/m for neat fat, and fat containing 18:1 and 16:0, respectively. It
312 can be argued that SC which stabilizes emulsions is at least partially displaced by these
313 two FAs, leading to lower surface tensions and thus smaller average diameters.

314 For any surface-active species, the mass, *m*, required to fully cover the fat/water
315 interface is given by the following relationship:

316 $$m = \Gamma \frac{6 m_{AMF}}{D_S \rho_{AMF}}$$ Equation (2)

317 where Γ is the surface coverage, m_{AMF} is the AMF mass and ρ_{AMF} is the AMF density
318 (0.92 g/cm^3). For SC, Γ is close to 1.2 mg/m^2 (Robson and Dalgleish, 1987). Thus, for the
319 emulsion with smallest average diameter homogenized at 500 bars, the amount of SC
320 adsorbed at the interface represents about 34% of the mass initially introduced. This
321 indicates that the protein concentration is, in any case, sufficient to saturate the interface
322 generated by the emulsification process.

323 Assuming that the surface coverage of 16:0 is Γ= 1.70 mg/m² (equivalent to 25
324 Å²/molecule) (Karleskind, 1992) and considering the average diameters D_s reported on
325 Table 1, from Eq. 2, we can estimate that the interface mobilizes at the most 15%, 34%
326 and 99% of the initial amount of this surfactant in LD, MD and SD emulsions, respectively.
327 16:0 is thus expected to localize at both the water/oil interface and in the volume of the
328 fat drops. The same statement holds for 18:1. Assuming Γ= 1.65 mg/m² (28.6
329 Å²/molecule) (Karleskind, 1992), the interface mobilizes at the most 14%, 34% and 97%
330 of this surfactant in LD, MD and SD emulsions, respectively.

331 Coalescence of the drops, if any, is supposed to increase the average diameter of
332 the emulsions and an evolution of the thermograms would then be expected. The size
333 distributions of emulsions stored at 4 °C for 48 h and rewarmed at room temperature were
334 measured and were strictly identical to those obtained right after emulsification (Results

335 not shown). Thus, for any emulsion, it can be stated that variations in thermal profiles
336 over time are not due to a change in droplet size distribution.
337
338 *3.2 Non-isothermal crystallization following a controlled cooling ramp*
339 *3.2.1 Neat AMF*
340 Crystallization of emulsions following a controlled ramp at -5 °C/min between 60
341 and 4 °C, was studied by DSC and compared to bulk AMF crystallized at the same rate
342 (Figure 1). Such approach allows to reveal supercooling effects induced by the dispersion
343 of matter, with a shift of the exothermic signal to lower temperatures as the size of the
344 drops decreases.
345 The onset crystallization temperature, T_{onset}, of bulk AMF is equal to 18.4 ± 0.9 °C.
346 As the average droplet size of the emulsions decreases from 6.0 to 0.8 μm, T_{onset}
347 significantly shifts from 15.7 ± 0.2 °C to 12.4 ± 0.4 °C (Figure 1, Table 2). This observation
348 about the impact of emulsification and of the droplet size is consistent with previous
349 studies (Michalski et al., 2004; Lopez et al., 2002; Truong, Bansal, Sharma, Palmer, &
350 Bhandari, 2014). The dispersion of fat in drops leads to its confinement. The substrates
351 of heterogeneous nucleation initially present in bulk AMF are therefore also confined in
352 the drops. Once the nucleation stage is overcome, crystal growth is limited by the finite
353 extension of the drops. This explains the higher degree of supercooling in emulsions
354 compared to bulk AMF. In addition, for the same fat fraction, when the average diameter
355 of the drops decreases, substrates of heterogeneous nucleation are increasingly
356 confined, *i.e.* the volume fraction of the drops that contain them decreases, which
357 necessarily slows down crystallization.
358 The number of DSC peaks and their position are also influenced by the
359 emulsification and by the size of the drops (Figure 1). In Table 2, we report the position

of the most intense ones. At a cooling rate of -5 °C/min, bulk AMF crystallizes following a two-stage process, and the corresponding peaks are centered at 17.2 °C and 11.4 °C. The thermogram obtained for LD emulsion exhibits 3 peaks: a low-amplitude event around 14 °C and two peaks centered at 12.5 °C and 8.6 °C. For MD emulsion, the thermal profile comprises a main peak centered at 8.6 °C, with a low-intense shoulder at higher temperatures. Finally, the thermogram of SD emulsion contains a single peak centered at 7.3 °C. To sum up, reducing the size of the drops in emulsions has the effect of directing crystallization towards a single thermal event. In submicron SD emulsion, the different AMF molecular fractions no longer crystallize separately as in bulk phase or in large droplets, but jointly.

In bulk AMF, crystalline growth preferentially results from the accretion of triglycerides with similar molecular size and shape. The crystallization process segregates triglycerides according to the chain length of their esterified FAs and their saturation level (Lavigne and Ollivon, 1997; Lopez, 2020). Therefore, several exothermic peaks are observed, each corresponding to a different molecular fraction, generally referred to as low-, middle- and high-melting TAGs. Conversely, in MD and SD emulsions, crystal growth generates mixed crystals involving different molecules, formed during a single and more intense exothermic event, reflecting a loss in molecular selectivity. Within a single droplet, the diffusion-limited process ensuring crystal growth is limited by the finite extension of the drops and molecules with similar molecular structure are quickly depleted. In the meanwhile, the expansion of the supercooling domain (lower T_{onset}) tends to diversify triglycerides available for adsorption on the growing crystalline faces. It can be assumed that fast crystallization in emulsions promotes growth in the α polymorphic form which is loose enough to allow the incorporation of triglycerides of different chain lengths.

385

386 *3.2.2. Impact of the modulators*

387 All systems containing modulators are compared to control emulsions containing
388 neat emulsified AMF.

389 The thermal profiles obtained for the emulsions with and without 3:0 at 0.5 wt% in
390 AMF are similar (Figure 2-A). For a given droplet size, comparable exothermic enthalpies,
391 centered on the same temperatures are obtained (Table 2). Bayard et al. (2017) showed
392 that 3:0 has an inhibitory effect on bulk AMF crystallization. They used pulsed low-
393 resolution nuclear magnetic resonance (p-NMR) to measure the solid fat content (SFC)
394 following a fast quench from 80 °C to 25 °C. AMF crystallization exhibited a sigmoidal
395 curve with an induction time followed by a sudden SFC increase whose average slope
396 was indicative of a steady crystallization process. The induction time was defined as the
397 delay between the start of the quench and the onset of the SFC signal. The addition of
398 3:0 at 1 wt% in AMF had the effect, among others, to considerably prolong the induction
399 time for crystallization and to slightly decrease the final SFC value. The inhibiting effect
400 was explained as being mainly due to the entropy of mixing. The presence of a low
401 molecular weight solute tends to lower the melting temperature following Raoult's law
402 (Atkins & Paula, 2014). In the present study, the partition of 3:0 between the oil droplets
403 and the aqueous phase makes the impact on AMF crystallization negligible.

404

405 Figure 2-B shows the evolution of the heat flow for emulsions based on 18:1 at 2.5
406 wt% in AMF. This modulator was shown to exhibit an inhibitory effect in bulk AMF by p-
407 NMR, revealed by a higher induction time and a lower maximal crystallization rate
408 compared to plain AMF (Bayard et al., 2017). The second crystallization peak, centered
409 around 12.5 °C for AMF emulsion, disappears in the presence of 18:1. Decreasing the

410 droplet size shifts the single crystallization peak to lower temperatures compared with
411 neat AMF (Table 2), revealing the supercooling effect of 18:1.The TAG fraction involved
412 in this large exothermic peak crystallizes at lower temperatures, together with a lower
413 melting fraction, probably forming mixed crystals. Two hypotheses can be drawn to
414 explain the origin of these observations:
415 - Interfacial effect. A fraction of 18:1 is adsorbed at the oil/water interface where it
416 forms a brush of chains oriented towards the oil phase. The disorder induced by the
417 double bond in *cis* configuration makes the brush structure incompatible with the ordered
418 packing of saturated AMF chains. As the average diameter decreases, the interfacial
419 surface area of the drops is augmented and the inhibitory effect of 18:1 becomes
420 increasingly pronounced.
421 - Volume effect. As in the continuous phase, 18:1 hinders the formation of crystal
422 nuclei (Bayard et al., 2017). Nucleation being the kinetically determining step, the
423 inhibitory effect of 18:1 is amplified when the volume of the drops decreases.
424
425 Figure 2-C corresponds to emulsified systems containing 16:0 at 2.5 wt% in AMF.
426 For the 3 sizes, the presence of 16:0 significantly increases T_{onset} compared to the control
427 emulsion (Table 2). The promoting effect of 16:0 in emulsified systems is consistent with
428 what was observed in bulk AMF by p-NMR, *i.e.* a lower induction time and a higher
429 maximal crystallization rate (Bayard et al., 2017). Moreover, the final SFC was not
430 affected by the addition of 16:0 (Bayard et al., 2017). The addition of 16:0 leads to new
431 exothermic events. In MD emulsion, a peak centered at 8.8 °C and a weak exothermic
432 signal between 18 °C and 14 °C appear, while the control emulsion shows a single
433 crystallization peak. For SD emulsion, a thermal event, not very intense and quite broad,
434 is distinguishable around 13 °C. Those new events suggest that 16:0 favors a segregation

435 of TAGs, with different fractions crystallizing separately. The value of T_{onset} obtained with
436 16:0 for the 3 emulsions slightly varies from 17 to 18 °C depending on the average droplet
437 size (Table 2). This result suggests that nucleation is no longer hindered by the decrease
438 in drop size. It can be assumed that 16:0 accelerates nucleation by acting through the
439 oil/water interfaces, where it concentrates. Saturated chains of 16:0 would crystallize at
440 the interface and would promote crystallization by acting as templates. It is well known
441 that crystal growth is favored if the alkyl chains within the nuclei are of similar length to
442 those of the main fraction of the fat (Basso et al., 2010). The templating effect can be due
443 to the fact that 16:0 chains are abundant in AMF. Since the amount of interface becomes
444 larger in finer emulsions, nucleation does not require deeper supercooling anymore.
445 Nevertheless, a mode of action *via* the core of the drops cannot be discarded. Indeed,
446 the amphiphilic nature of 16:0 may allow this FA to self-assemble in the melted fat. Due
447 to the stacking of the aliphatic chains, the structures resulting from the self-assembly
448 would constitute numerous nucleation sites. Reverse micelles with the hydrophobic
449 "brush" facing the oil phase can potentially be formed and may accelerate nucleation
450 (McClements, 2004).
451
452 To better understand the extent to which the interfacial and bulk properties of 16:0
453 are involved in accelerating AMF crystallization, the impact of 16:0 was compared to that
454 of PPP which is not surface-active, while comprising the same FA chain. Emulsions
455 containing 16:0 or PPP were prepared at 5 wt% in AMF. Their thermal profiles are
456 presented in Figure 2-D. The modulator content is higher than previously, which will allow
457 in the meanwhile to assess the influence of the modulator concentration.
458 Doubling 16:0 concentration greatly modifies the AMF crystallization profile
459 (Figures 2-C and 2D). Regardless of the droplet size, an increase in T_{onset} is observed

460 (Table 2). In addition, crystallization involves only one mean intense peak, instead of the
461 two peaks observed at lower 16:0 concentration. Since the size distributions are
462 comparable for both concentrations, it may be concluded that a high 16:0 concentration
463 promotes AMF crystallization in the droplets core.

464 For LD emulsion, substitution of 16:0 by PPP induces a significant change in the
465 thermal pattern with the appearance of a new peak centered at 14 °C, nearly 3 °C above
466 the main peak of AMF+16:0 and a shoulder around 17 °C (Figure 2-D). A second peak,
467 less intense, is centered around 8 °C (this peak was already present in the control
468 emulsion). For SD emulsion, PPP shifts the main crystallization peak by + 2.4 °C
469 compared to the emulsion based on neat AMF. An intermediate pattern is observed for
470 MD emulsion. Irrespectively of the droplet size, PPP modulates the crystallization by
471 increasing T_{onset}.

472 To further assess the origin of the promoting effect of 16:0 and PPP, a 15 µL drop
473 of AMF, melted at 80 °C, was formed in a 0.33% SC solution, thermostatically controlled
474 at 25 °C in a rising drop tensiometer. Figure 3-A shows a sampling of the acquired images.
475 As the crystals form, they prevent light from passing through the fat phase, causing dark
476 spots to appear in the drop. This experiment confirms that 16:0 and PPP are
477 crystallization promoters, as drops containing them darken faster than the control system
478 based on neat AMF. It also allows to appreciate the shape, size and number of crystals
479 and to see where they preferentially form, in the drop core or at the interface. Figure 3-B
480 shows a magnification of the images obtained after 12 minutes of crystallization. The
481 control drop does not yet show any crystal, while the first crystals are visible in the
482 presence of 16:0 and PPP. The crystals in the drop containing PPP tend to form a
483 sediment (indicated by the arrow). In Figure 3-A, at times between 24 and 36 min, the
484 upper part of the drop appears slightly less turbid than the lower part, again reflecting

485 crystals sedimentation. On the other hand, in the presence of 16:0 (Figure 3-B), the
486 crystals formed remain attached to the water/oil interface and the blackening of the drop
487 is spatially homogeneous (Figure 3-A). This blackening is also faster than in the drop
488 containing PPP. The crystals form a thick layer at the interfaces and thus opacify the drop
489 rapidly. This experiment supports the conclusion that 16:0 accelerates crystallization *via*
490 the interface, while PPP acts *via* the core of the drop.

491 From the whole set of observations, it can be concluded that different promoting
492 mechanisms are at play for these two modulators:

493 - Crystallization of 16:0 occurs first at the interfaces, where it tends to adsorb and
494 pack due to its amphiphilic nature. The finer the drops, the greater the amount of interface
495 and thus the fraction of adsorbed 16:0, which could justify the increase in intensity of the
496 early exothermic peak (Figure 2-D). However, the increasing curvature may hinder
497 crystallization since the peak maximum shifts towards lower temperatures as the drop
498 size decreases. T_{onset} tends to increase with the concentration of 16:0 in AMF, presumably
499 due to an increase of the interfacial concentration of this modulator. Nevertheless, a
500 volume effect cannot be excluded since the concentration of free 16:0 in the core of the
501 drops is also likely to increase, especially in emulsions with large average droplet
502 diameter.

503 - PPP crystallizes concomitantly with a fraction of high-melting AMF TAGs. It has
504 been shown that adding PPP at low concentration does not modify the nanostructure of
505 AMF crystals (Bayard et al., 2021). This modulator would mobilize saturated AMF TAGs
506 comprising comparable chain lengths to form mixed crystals. The expansion of the
507 supercooling domain (decrease of T_{onset}) as the average droplet size decreases gives a
508 hint that that its effect has a bulk (volume) origin.

509

510 *3.3 Melting behavior of emulsions after isothermal crystallization at 4 °C for 90 min and*
511 *48 h*

512 *3.3.1 Neat AMF*

513 Following the crystallization ramp at -5 °C/min, the samples reached the target
514 temperature, 4 °C, after 11 min and were subjected to a short (90 min) isothermal period
515 at this temperature. Alternatively, samples were quenched from 60 °C to 4 °C in
516 approximately 2-3 min and were stored for 48 h at 4 °C in a thermostatically controlled
517 chamber. The crystallization state was then characterized by DSC following a melting
518 ramp at +5 °C/min. In Figure SI3 (supplementary information), the thermal melting profiles
519 for the 3 emulsions are superimposed for the 2 cold storage times: 90 min (A) and 48 h
520 (B). Crystallization keeps on between these 2 storage periods, as evidenced by the
521 overall heat flow observed in the thermograms between 4 °C and 15 °C which is lower
522 after 48 h of crystallization than after 90 min. For instance, an intense endothermic peak
523 around 21 °C, not observed after 90 min, is present after 48 h. This reflects an evolution
524 of the crystals from a less stable form (melting between 4 and 15 °C) at short times, to
525 more stable forms (melting around 21 °C) when the isothermal period becomes longer. It
526 is likely that the medium melting fraction of AMF undergoes a polymorphic transition
527 between 90 min and 48 h of crystallization. In the remainder, we will mainly comment the
528 results obtained after 48 h of storage for both AMF and AMF+modulator systems.

529 Whatever the average droplet size, the melting profiles of AMF emulsions stored
530 for 48 h at 4 °C exhibit 3 endothermic events (Figure 4 and Figure SI4 in supplementary
531 information):

532 - A peak at temperatures below 15 °C, reflecting the fusion of the most unstable
533 forms, probably 3L-α forms (Michalski et al., 2004);

534 - An intense peak between 15 °C and 25 °C, attributable to the melting of 3L and
535 2L α and β' forms (Lopez et al., 2001b);
536 - A thermal event around 26 °C that would correspond to the melting of a 2L-β'
537 form (Michalski et al., 2004). This event is more apparent on the thermograms of LD and
538 MD emulsions. The curvature and confinement imposed by the submicron-sized drops in
539 SD emulsion inhibit the polymorphic transition leading to the formation of this crystals
540 fraction.
541
542 *3.3.2 Impact of the modulators*
543 The melting profiles obtained after 48 h at 4 °C, for the 3 droplet sizes (Figure 4-
544 A) show that the emulsions with and without 3:0 exhibit similar enthalpic behaviors, again
545 suggesting that this modulator initially dissolved at 0.5 wt% has no impact on the
546 formation of the polymorphs, mainly because of its high-water solubility. Likewise, the
547 endothermic peaks with and without 18:1 are quite close (Figure 4-B, Table 2). The
548 melting profiles are weakly modified by the presence of 16:0 at 2.5 wt% in AMF (Figure
549 4-C, Table 2). Thus, after a sufficiently long crystallization time, the unstable polymorphs
550 formed at short times evolve towards more stable ones, regardless of the drop size.
551
552 Both 16:0 and PPP at 5 wt% in AMF lead to the appearance of endothermic peaks
553 at temperatures higher than those of the control (Figure 4-D, Table 2). For 16:0, a weak
554 endothermic event is observed between 35 °C and 40 °C in LD emulsion and between
555 35 °C and 47 °C in MD emulsion. For PPP, the melting range of AMF extends to about
556 45 °C, a variation of +10 °C in T_{offset} compared to neat AMF. The heat flow is significant
557 between 35 °C and 45 °C. The enthalpy of fusion in this range cannot be due to PPP
558 alone. Indeed, in Figure SI5 (supplementary information), we show the signal obtained

559 for LD emulsion as well as its integral from 4 to 55 °C. The SFC of bulk AMF is 52% at
560 4 °C (Bayard et al., 2017). Assuming that PPP is fully crystallized, the expected fraction
561 of the enthalpic signal between 35 °C and 45 °C should represent about 10% of the
562 cumulative signal, which is half of the actual value obtained in Figure SI5. In addition, this
563 signal appears in the continuity of thermal events occurring at lower temperatures and
564 not as an individual peak. It can be concluded that this endothermic heat flow corresponds
565 to the melting of mixed crystals comprising PPP and AMF TAGs. Conversely, in the
566 system containing 16:0, the isolated peak at high temperature, around 40 °C, and its low
567 intensity suggest that the signal is due to the melting of 16:0 alone, which would be
568 segregated from the rest of the fat. The melting temperature of pure 16:0 is 63 °C, but in
569 the presence of liquid oil, the entropy of mixing lowers its melting temperature.
570
571 *3.4 Analysis of the phase change enthalpies*
572 A detailed analysis of the total phase change enthalpy ΔH between 4 and 45 °C
573 (Table 2) was carried out with the aim of assessing the crystallization kinetics. Figure SI6-
574 A and B (supplementary information) display the average values obtained with neat AMF
575 and with all samples including neat AMF and AMF+modulators, respectively. We consider
576 the absolute value of the crystallization enthalpy, $\Delta H_{cryst,}$ measured following a cooling
577 ramp in order to facilitate its comparison with the melting enthalpies measured after a
578 storage of 90 min, ΔH_{90min}, and 48 h, ΔH_{48h}. The crystallization enthalpy is lower than the
579 melting enthalpies. This can be explained by the fast cooling that occurred in 11 minutes,
580 resulting in partial crystallization, and by the formation of metastable polymorphs, whose
581 enthalpies are known to be lower than those of stable ones (Ravotti, Worlitschek, Pulham,
582 & Stamatiou, 2020). After a given storage time, with only a few exceptions, the total
583 melting enthalpies follow the same hierarchy: $\Delta H_{LD} > \Delta H_{MD} > \Delta H_{SD}$.

584 All other factors being equal, the average values obtained with AMF alone and with
585 all samples are almost identical (the differences between figures SI6-A and B are not
586 statistically significant). The modulators modify the crystallization scenario at short times
587 as revealed by the thermograms reported in Figures 2, 4 and SI4 but the global enthalpy
588 is a "mean field" parameter that does not allow to differentiate the impact of the
589 modulators.

590 Crystallization still evolves after 90 minutes. This can be concluded after noticing
591 that ΔH_{90min} is lower than ΔH_{48h}. Several factors may explain this lower enthalpy: (i) a
592 lower solid content; (ii) the presence of metastable forms with lower melting enthalpy than
593 more stable polymorphs formed during storage; (iii) transitions towards more stable forms
594 during fusion trigger an exothermic signal that lowers the total enthalpy (Figure SI4).

595 After 48 h, it is not clear whether a steady state has been reached. The enthalpy
596 of SD emulsions remains significantly lower than in the other 2 emulsions. It can be
597 argued that the crystallization kinetics is slower in SD emulsion. However, an alternative
598 interpretation can be put forward. According to the classical theory of homogeneous
599 nucleation, the Gibbs energy difference associated to the formation of a solid germ from
600 liquid molecules comprises a volume (bulk) term linked to the difference in the standard
601 chemical potential of liquid and solid phases and an interfacial contribution accounting for
602 solid-liquid interfacial tension (Abraham, 1974). Within this model, the growth of a germ
603 leading to crystal formation is only possible if it forms spontaneously with a size larger
604 than a critical threshold value, r*. It can be hypothesized that the confinement in very tiny
605 droplets modifies the thermodynamic conditions. Grossier and Veesler (2008) have
606 calculated the change in free energy associated to the formation of a nucleus containing
607 solute molecules in a supersaturated finite system (droplet). As the nucleus grows, solute
608 molecules in the liquid phase are depleted, which tends to reduce supersaturation.

609 Because of this, at low initial supersaturations, it is impossible for a critical nucleus to
610 form. A critical nucleus can form only if supersaturation exceeds a threshold value. In this
611 case, once the critical size has been reached, the nucleus continues to grow until it
612 reaches a second critical size associated with a potential well in the energy curve. Growth
613 beyond this “equilibrium” size is not favored. These thermodynamic effects can therefore
614 limit the size that a nucleus can attain within a finite reservoir like tiny droplets, or can
615 even prevent nucleation from supersaturated or undercooled solutions that would yield
616 crystals in bulk conditions.
617
618 **4. Conclusion**
619 In this paper, we studied the impact of confinement and of the presence of
620 additives on the crystallization and melting of milk fat. Differential scanning calorimetry
621 was used to assess the kinetics and the nature of thermal events occurring during
622 crystallization under non-isothermal and isothermal conditions. The impact of
623 confinement was addressed by fabricating oil-in-water emulsions and by tuning their
624 average drop size. Upon cooling, in the absence of additives, the crystallization onset
625 temperature tended to decrease as the average drop size was reduced. In addition to this
626 effect usually observed in emulsions based on crystallizable oils, we showed that unstable
627 crystals formed in the early stages and that crystallization was uncomplete even after 48
628 h of low temperature storage in submicron emulsions.
629 Additives likely to be formed in dairy processes, propionic, palmitic and oleic acids
630 or added like tripalmitin were dissolved in milk fat at a concentration less than or equal to
631 5%. In emulsions, propionic acid showed no effect. Due to its high polarity, this additive
632 was transferred to a large extent in the aqueous phase. Oleic acid favored supercooling
633 and promoted unstable forms in the early stages of crystallization but its impact became

634 insignificant after 48 h of cold isothermal storage. Two crystallization promoters, palmitic
635 acid and tripalmitin, were also studied. The impact of palmitic acid was related to its
636 interfacial (amphiphilic) properties and vanished considerably after 48 h. Conversely,
637 tripalmitin influenced crystallization *via* volume effects that were persistent. It formed
638 mixed crystals which considerably extended the melting range of the milk fat.

639 We hope the results provided in this article will provide a useful guidance for
640 mastering crystallization in dairy products.

641

642 **Acknowledgements**

643 The authors acknowledge the French National Association of Technical Research
644 (ANRT) for its financial support through a Ph.D. research grant for M.B.

Table Captions

Table 1: Average diameter and polydispersity of AMF-in-water emulsions with and without modulators obtained at various homogenization pressures.

Table 2: Characteristic temperatures and enthalpies of AMF-in-water emulsions with and without modulators obtained at various homogenization pressures. All data derive from DSC experiments.

Figure captions

Figure 1: DSC crystallization thermograms of bulk AMF and of AMF-in-water emulsions following a controlled cooling ramp from 60 °C to 4 °C at -5 °C/min. Heat flows are related to the mass of AMF contained in the sample. Thermograms are off set vertically for clarity.

Figure 2: DSC crystallization thermograms of emulsions containing various modulators following a controlled cooling from 60 °C to 4 °C at -5 °C/min. The thermogram of the emulsion comprising neat AMF is provided for comparison.

Figure 3: A: Images of AMF drops (15 μL) during crystallization at 25 °C. From left to right: neat AMF (control), AMF+0.25 wt% PPP; AMF+0.25 wt% 16:0. B: Focus on time t=12 min. Each of the modulators was added in molten AMF.

Figure 4: DSC melting thermograms of emulsions containing various modulators measured after 48 h of isothermal storage at 4 °C. The thermogram of the emulsion comprising neat AMF is provided for comparison.

670 **Supplementary data captions**

671 Figure SI1: Thermal programs implemented to assess the evolution of fat crystallization
672 under dynamic (cooling, solid line) and static (isothermal, dotted line) conditions.

673

674 Figure SI2: (A) Micrographs of neat AMF-in-water emulsions obtained at various
675 homogenization pressures. The emulsions were diluted prior to the observation. The
676 scale bar represents 50 μm. (B) Size distribution of AMF-in-water emulsions with and
677 without modulators obtained at various homogenization pressures; the darkest lines
678 correspond to neat AMF; in the bottom graph, the lightest lines correspond to PPP and
679 those with intermediate intensity correspond to 16:0.

680

681 Figure SI3: Melting thermograms after 90 min (A) and 48 h (B) of isothermal storage at
682 4 °C of neat AMF-in-water emulsions of various average diameters.

683

684 Figure SI4: DSC melting thermograms of emulsions containing various modulators
685 measured after 90 min of isothermal storage at 4 °C. The thermogram of the emulsion
686 comprising neat AMF is provided for comparison.

687

688 Figure SI5: DSC thermogram of LD emulsion following a ramp at +5 °C/min after
689 isothermal storage at 4 °C for 48h. The fat phase contains 5 wt% PPP in AMF. Left axis:
690 heat flow; right axis: cumulative curve (enthalpy).

691

692 Figure SI6: Crystallization and melting enthalpies of (A) emulsions based on neat AMF
693 and (B) all emulsions comprising neat AMF and AMF+modulators. The values reported
694 here are averaged over all data provided in Table 2.

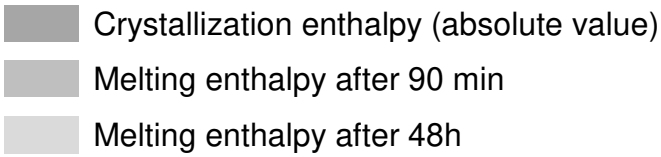

695

696 Mean values under the vertical bars are significantly different ($p < 0.05$) using a one-way

697 analysis of variance followed by a pairwise t-test.

698

699 **References**

700 Atkins, P. & de Paula, J. (2014). *Atkins' Physical Chemistry*. *(8th Edition) Oxford*
701 *University Press, Oxford.*

702 Basso, R. C., Ribeiro, A. P. B., Masuchi, M. H., Gioielli, L. A., Gonçalves, L. A. G.,
703 dos Santos, A. O., Cardoso, L.P., & Grimaldi, R. (2010). Tripalmitin and
704 monoacylglycerols as modifiers in the crystallisation of palm oil. *Food Chemistry*, *122*(4),
705 1185–1192. https://doi.org/10.1016/j.foodchem.2010.03.113.

706 Bayard, M., Kauffmann, B., Leal-Calderon, F. & Cansell. M. (2021). Isothermal
707 crystallization of anhydrous milkfat in presence of free fatty acids and their esters: From
708 nanostructure to textural properties. *Food Chemistry*, in press.
709 https://doi.org/10.1016/j.foodchem.2021.130533.

710 Bayard, M., Leal-Calderon, F., & Cansell, M. (2017). Free fatty acids and their
711 esters modulate isothermal crystallization of anhydrous milk fat. *Food Chemistry, 218,*
712 22–29. https://doi.org/10.1016/j.foodchem.2016.09.042.

713 Bayés-García, L., Patel, A. R., Dewettinck, K., Rousseau, D., Sato, K., & Ueno, S.
714 (2015). Lipid crystallization kinetics - Roles of external factors influencing functionality of
715 end products. *Current Opinion in Food Science, 4*, 32–38.
716 https://doi.org/10.1016/j.cofs.2015.04.005.

717 Bell, G.H. (1973). Solubilities of normal aliphatic acids, alcohols and alkanes in
718 water. *Chemistry and Physics of Lipids*, 10(1), 1–10. https://doi.org/10.1016/0009-
719 3084(73)90036-4.

720 Bibette, J., Leal-Calderon, F., Schmitt, V., & Poulin, P. (2002). *Springer Tracts in*
721 *modern Physics: Emulsion Science. Basic principles. An overview*. Springer-Verlag:
722 Berlin.

De Feijter, J.A., Benjamins, J., & Tamboer, M. (1987). Adsorption displacement of proteins by surfactants in oil-in-water emulsions. *Colloids and Surfaces, 27(4)*, 243-266. https://doi.org/10.1016/0166-6622(87)80145-2.

Demetriades, K, McClements, DJ. (2000). Influence of sodium dodecyl sulfate on the physicochemical properties of whey protein-stabilized emulsions. *Colloids and Surfaces A: Physicochemical and Engineering Aspects*, *161*, 391-400. https://doi.org/10.1016/S0927-7757(99)00210-1.

Dickinson, E. (2012). Emulsion gels: The structuring of soft solids with protein-stabilized oil droplets. *Food Hydrocolloids*, *28*, 224–241. https://doi.org/10.1016/j.foodhyd.2011.12.017.

Foubert, I., Vanhoutte, B., & Dewettinck, K. (2004). Temperature and concentration dependent effect of partial glycerides on milk fat crystallization. *European Journal of Lipid Science and Technology*, *106*(8), 531–539. https://doi.org/10.1002/ejlt.200400979.

Fredrick, E., Walstra, P., & Dewettinck, K. (2010). Factors governing partial coalescence in oil-in-water emulsions. *Advances in Colloid and Interface Science*, *153*(1,2), 30–42. https://doi.org/10.1016/j.cis.2009.10.003.

Romain Grossier, R., & Veesler, S. (2009). Reaching one single and stable critical cluster through finite-sized systems. *Crystal Growth & Design*, *9*(4), 1917–1922. https://doi.org/10.1021/cg801165b.

Karleskind, A. (1992). *Manuel des corps gras. Vol.1*. Paris; Londres; New York: Technique et Documentation-Lavoisier.

Kaufmann, N., Kirkensgaard J. K., Andersen, U., & Wiking, L. (2013). Shear and rapeseed oil addition affect the crystal polymorphic behavior of milk fat. *Journal of the*

747 *American Oil Chemists' Society*, *90*, 871–880. https://doi.org/10.1007/s11746-013-2226-
748 z.
749 Lavigne, F. & Ollivon, M. (1997). Milk fat and its fractions. *Oléagineux, Corps gras,*
750 *Lipides, 4(3),* 212–219.
751 Lopez C. (2020). Crystallization and melting properties of milk fat*. In: Truong, T.,*
752 *Lopez, C., Bhandari, B., Prakash, S. (eds), Dairy Fat Products and Functionality.*
753 Springer, International Publishing.
754 Lopez, C., Bourgaux, C., Lesieur, P., Bernadou, S., Keller, G., & Ollivon, M. (2002).
755 Thermal and structural behavior of milk fat. 3. Influence of cooling rate and droplet size
756 on cream crystallization. *Journal of Colloid and Interface Science, 254(1)*, 64–78.
757 https://doi.org/10.1006/jcis.2002.8548.
758 Lopez, C., Lavigne, F., Lesieur, P., Keller, G., & Ollivon, M. (2001a). Thermal and
759 structural behavior of anhydrous milk fat. 2. Crystalline forms obtained by slow cooling.
760 *Journal of Dairy Science, 84(11)*, 2402–2412. https://doi.org/10.3168/jds.S0022-
761 0302(01)74689-9.
762 Lopez, C., Lesieur, P., Bourgaux, C., Keller, G. & Ollivon, M. (2001b). Thermal and
763 structural behavior of milk fat: 2. Crystalline forms obtained by slow cooling of cream.
764 *Journal of Colloid and Interface Science, 240(1)*, 150–161.
765 https://doi.org/10.1006/jcis.2001.7664.
766 Martini, S., Herrera, M. L., & Hartel, R. W. (2002). Effect of cooling rate on
767 crystallization behavior of milk fat fraction/sunflower oil blends. *Journal of the American*
768 *Oil Chemists' Society, 79,* 1055–1062.
769 McClements, D.J. (2004). *Food emulsions: principles, practices, and techniques*
770 (2nd ed.). *CRC Press, Boca Raton.* https://doi.org/10.1201/9781420039436.

771 McClements, D. J. (2012). Crystals and crystallization in oil-in-water emulsions:
772 Implications for emulsion-based delivery systems. *Advances in Colloid and Interface*
773 *Science*, *174(15)*, 1–30. https://doi.org/10.1016/j.cis.2012.03.002.
774 Metin, S. & Hartel, R. W. (2005). Crystallization of fats and oils. *In F. Shadidi (Ed.)*
775 *(Sixth edition), Bailey's Industrial Oil and Fat Products* (pp. 45–76). John Wiley & Sons,
776 Inc.
777 Michalski, M.-C., Ollivon, M., Briard, V., Leconte, N., & Lopez, C. (2004). Native fat
778 globules of different sizes selected from raw milk: thermal and structural behavior.
779 *Chemistry and Physics of Lipids*, *132*, 247–261.
780 https://doi.org/10.1016/j.chemphyslip.2004.08.007.
781 Patel, A. R. & Dewettinck, K. (2015). Current update on the influence of minor lipid
782 components, shear and presence of interfaces on fat crystallization. *Current Opinion in*
783 *Food Science, 3,* 65–70. https://doi.org/10.1016/j.cofs.2015.05.010.
784 Ravotti, R., Worlitschek, J., Pulham, C. R., & Stamatiou, A. (2020). Triglycerides
785 as novel phase-change materials: a review and assessment of their thermal properties.
786 *Molecules*, *25*(23), 5572–5598. https://doi:10.3390/molecules25235572.
787 Robson, E. W. & Dalgleish, D.G. (1987). Interfacial composition of sodium
788 caseinate emulsions. *Journal of Food Science*, *52*(6), 1694–1698.
789 Rønholt, S., Mortensen, K., & Knudsen, J. C. (2013). The effective factors on the
790 structure of butter and other milk fat-based products. *Comprehensive Reviews in Food*
791 *Science and Food Safety*, *12*(5), 468–482. https://doi.org/10.1111/1541-4337.12022.
792 Sato, K. (1999). Solidification and phase transformation behaviour of food fats - a
793 review. *Lipid / Fett*, *101*(12), 467–474.

794 Sato, K., Bayés-García, L., Calvet, T., Cuevas-Diarte, M. À., & Ueno, S. (2013).
795 External factors affecting polymorphic crystallization of lipids. *European Journal of Lipid*
796 *Science and Technology*, *115*(11), 1224–1238. https://doi.org/10.1002/ejlt.201300049.
797 Sato, K. & Ueno S. (2011). Crystallization, transformation and microstructures of
798 polymorphic fats in colloidal dispersion states. *Current Opinion in Colloid and Interface*
799 *Science*, *16(5)*, 384–390. https://doi.org/10.1016/j.cocis.2011.06.004.
800 Smith, K. W., Bhaggan, K., Talbot, G., & Malssen, K. (2011). Crystallization of fats:
801 Influence of minor components and additives. *Journal of the American Oil Chemists'*
802 *Society, 88,* 1085–1101. https://doi.org/10.1007/s11746-011-1819-7.
803 Talbot, G., Smith, K., & Bhaggan, K. (2012). Influence of minor components on fat
804 crystallization. *Lipid Technology, 24,* 83–85. https://doi.org/10.1002/lite.201200180.
805 ten Grotenhuis, E., van Aken, G. A., van Malssen, K. F., & Schenk, H. (1999).
806 Polymorphism of milk fat studied by differential scanning calorimetry and real-time X-ray
807 powder diffraction. *Journal of the American Oil Chemists' Society, 76*, 1031–1039.
808 https://doi.org/10.1007/s11746-999-0201-5.
809 Truong, T., Bansal, N., Sharma, R., Palmer, M., & Bhandari, B. (2014). Effects of
810 emulsion droplet sizes on the crystallisation of milk fat. *Food Chemistry*, *145*, 725–735.
811 https://doi.org/10.1016/j.foodchem.2013.08.072.
812 Vanhoutte, B., Dewettinck, K., Foubert, I., Vanlerberghe, B., & Huyghebaert, A.
813 (2002). The effect of phospholipids and water on the isothermal crystallization of milk fat.
814 *European Journal of Lipid Science and Technology*, *104*(8), 490–495.
815 https://doi.org/10.1002/1438-9312(200208)104:8<490::AID-EJLT490>3.0.CO;2-U.
816 Walstra, P., Wouters, J. T. M., & Geurts, T. J. (2006). *Dairy science and technology*
817 *(2nd ed),* CRC/Taylor & Francis, Boca Raton.

Wright, A. J., Hartel, R. W., Narine, S. S., & Marangoni, A. G. (2000). The effect of minor components on milk fat crystallization. *Journal of the American Oil Chemists' Society*, *77*(5), 463–475. https://doi.org/10.1007/s11746-000-0075-8.

Wright, A. & Marangoni, A. G. (2003). The effect of minor components on milk fat microstructure and mechanical properties. *Food Engineering and Physical Properties*, *68*(1), 182–186. https://doi.org/10.1111/j.1365-2621.2003.tb14137.x.

Tables

Table 1

	Homogenization pressure (bars)	*Emulsion*	D_v[1,4] (μm)	D_s[2,4] (μm)	*Polydispersity* [3,4] (%)
Neat AMF	0	Large	6.0 ± 0.2[a]	3.4 ± 0.1[a]	48 ± 1[a]
	50	Medium	2.2 ± 0.3[b]	1.3 ± 0.1[b]	63 ± 1[b]
	500	Small	0.8 ± 0.0[c]	0.5 ± 0.0[c]	80 ± 3[c]
AMF+ 0.5 wt% **3:0**	0	Large	6.2 ± 0.1[a]	3.6 ± 0.3[a]	48 ± 3[a]
	50	Medium	2.2 ± 0.0[b]	1.4 ± 0.0[b]	57 ± 2[b]
	500	Small	0.7 ± 0.0[c]	0.5 ± 0.0[c]	73 ± 2[c]
AMF+ 2.5 wt% **18:1**	0	Large	4.8 ± 0.1[a]	3.0 ± 0.5[a]	47 ± 4[a]
	50	Medium	2.2 ± 0.0[b]	1.3 ± 0.0[b]	61 ± 3[b]
	500	Small	0.7 ± 0.0[c]	0.4 ± 0.0[c]	75 ± 1[c]
AMF+ 2.5 wt% **16:0**	0	Large	4.4 ± 0.1[a]	2.9 ±0.1[a]	45 ± 3[a]
	50	Medium	2.2 ± 0.0[b]	1.3 ± 0.1[b]	61 ± 4[b]
	500	Small	0.7 ± 0.0[c]	0.5 ± 0.0[c]	71 ± 2[c]
AMF+ 5 wt% **16:0**	0	Large	4.3 ± 0.1[a]	2.7 ± 0.1[a]	48 ± 1[a]
	50	Medium	1.8 ± 0.2[b]	1.1 ± 0.1[b]	61 ± 2[b]
	500	Small	0.6 ± 0.0[c]	0.4 ± 0.0[c]	71 ± 6[c]
AMF+ 5 wt% **PPP**	0	Large	6.2 ± 0.1[a]	3.7 ± 0.2[a]	48 ± 2[a]
	50	Medium	2.7 ± 0.1[b]	1.6 ± 0.0[b]	64 ± 2[b]
	500	Small	0.8 ± 0.0[c]	0.6 ± 0.0[c]	78 ± 0[c]

[1] D_v: volume-averaged diameter $\frac{\sum N_i D_i^4}{\sum N_i D_i^3}$ where N_i is the total number of particles with diameter D_i

[2] D_s: surface-averaged diameter, $\frac{\sum N_i D_i^3}{\sum N_i D_i^2}$ where N_i is the total number of particles with diameter D_i

[3] *P*: polydispersity, $\frac{1}{\overline{D}} \frac{\sum N_i D_i^3 (\overline{D} - D_i)}{\sum N_i D_i^3}$ where $\overline{D}$ is the median diameter, *i.e.* the value for which the cumulative undersized volume fraction is equal to 50%, and N_i is the total number of particles with diameter D_i

[4] Values are expressed as mean ± standard deviations, n = 5 independent preparations. Within a column, mean values with unlike superscript letters are significantly different ($p < 0.05$) using a one-way analysis of variance followed by a pairwise t-test.

Table 2

Emulsion		Crystallization				Melting after 90 min				Melting after 48h		
		T_{onset}[1,4]	T_{peak}[2]		ΔH[3,4]	T_{peak}[2]		T_{offset}[1]	ΔH[3,4]	T_{peak}[2]	T_{offset}[1]	ΔH[3,4]
		°C	°C	°C	J/g of fat	°C	°C	°C	J/g of fat	°C	°C	J/g of fat
Neat AMF	bulk	18.4 ± 0.9	16.8 ± 0.3	10.2 ± 0.3								
	LD	15.7 ± 0.2$^{a\circ}$	12.5 ± 0.1$^{a\circ}$	8.6 ± 0.6	-37.1 ± 3.9$^{ab\circ}$	19.6 ± 0.5$^{a\circ}$	32.6 ± 0.4$^{a\circ}$	36.4 ± 0.3$^{a\circ}$	59.2 ± 9.6$^{a\circ}$	21.5 ± 0.5$^{a\circ}$	36.8 ± 0.3$^{a\circ}$	66.2 ± 12.8$^{a\circ}$
	MD	13.7 ± 0.9^{a*}	8.6 ± 0.7^{ab*}		-33.5 ± 3.1$^{ab\circ}$	14.9 ± 0.2^{a*}	31.6 ± 1.8$^{a\circ *}$	36.3 ± 0.5$^{a\circ}$	44.5 ± 7.5$^{a\circ}$	21.6 ± 0.2$^{a\circ}$	36.5 ± 0.1$^{a\circ}$	61.2 ± 3.3$^{a\circ}$
	SD	12.4 ± 0.4$^{a\#}$	7.3 ± 0.3$^{a\#}$		-23.8 ± 4.6^{ab*}	13.3 ± 0.3$^{a\#}$	30.5 ± 0.1^{a*}	36.1 ± 0.5$^{a\circ}$	41.4 ± 8.4$^{a\circ}$	21.7 ± 0.2$^{a\circ}$	36.5 ± 0.5$^{a\circ}$	53.3 ± 9.0$^{a\circ}$
AMF+ 0.5 wt% **3:0**	LD	15.1 ± 0.1^{a}	12.3 ± 0.1^{a}	8.6 ± 0.1^{a}	-32.8 ± 1.0^{a}	19.2 ± 0.5^{a}	33.4 ± 0.4^{a}	36.4 ± 0.3^{a}	52.6 ± 8.5^{a}	21.6 ± 0.5^{a}	36.0 ± 0.3^{a}	57.5 ± 11.1^{a}
	MD	13.4 ± 0.3^{a}	9.1 ± 0.7^{a}		-35.0 ± 1.4^{abc}	14.8 ± 0.2^{a}	31.0 ± 1.8^{a}	36.2 ± 0.5^{a}	46.2 ± 7.8^{a}	20.8 ± 0.2^{b}	36.2 ± 0.1^{a}	57.4 ± 3.1^{a}
	SD	11.5 ± 0.1^{a}	6.7 ± 0.4^{a}		-28.4 ± 0.5^{b}	13.4 ± 0.3^{a}	30.6 ± 0.1^{a}	36.2 ± 0.5^{a}	31.8 ± 6.5^{a}	21.6 ± 0.2^{a}	36.0 ± 0.5^{a}	44.1 ± 7.4^{a}
AMF+ 2.5 wt% **18:1**	LD	15.8 ± 0.1^{a}	9.0 ± 0.3^{d}		-36.5 ± 1.1^{ab}	15.2 ± 0.4^{b}	33.0 ± 0.4^{a}	36.0 ± 0.2^{a}	62.1 ± 10.1^{a}	21.0 ± 0.5^{a}	36.2 ± 0.3^{a}	64.1 ± 12.4^{a}
	MD	13.3 ± 0.4^{a}	7.6 ± 0.3^{b}		-30.6 ± 4.8^{b}	13.2 ± 0.2^{b}	33.0 ± 1.9^{a}	35.6 ± 0.5^{a}	41.2 ± 6.9^{a}	21.2 ± 0.2^{ab}	36.2 ± 0.1^{a}	51.8 ± 2.8^{b}
	SD	10.8 ± 2.5^{a}	4.7 ± 0.1^{b}		-21.8 ± 3.6^{a}	12.6 ± 0.3^{a}	30.0 ± 0.1^{a}	35.2 ± 0.5^{a}	34.9 ± 7.1^{a}	20.4 ± 0.2^{b}	35.6 ± 0.5^{a}	48.1 ± 8.1^{a}
AMF+ 2.5 wt% **16:0**	LD	17.0 ± 0.1^{b}	12.5 ± 0.1^{a}		-34.7 ± 4.1^{a}	13.0 ± 0.3^{c}	33.2 ± 0.4^{a}	35.8 ± 0.2^{a}	42.2 ± 6.8^{a}	21.0 ± 0.5^{a}	36.2 ± 0.3^{a}	52.2 ± 10.1^{a}
	MD	18.1 ± 0.1^{b}	12.5 ± 0.7^{c}	8.8 ± 0.1^{a}	-36.0 ± 2.8^{bc}	12.8 ± 0.2^{b}	32.8 ± 1.9^{a}	35.6 ± 0.5^{a}	38.7 ± 6.5^{a}	21.2 ± 0.2^{ab}	36.2 ± 0.1^{a}	64.3 ± 3.5^{a}
	SD	17.0 ± 1.4^{b}	4.7 ± 0.4^{b}		-27.2 ± 3.6^{ab}	12.6 ± 0.3^{a}	30.2 ± 0.1^{a}	34.8 ± 0.5^{a}	40.0 ± 8.1^{a}	20.8 ± 0.2^{b}	35.6 ± 0.5^{a}	49.7 ± 8.4^{a}
AMF+ 5 wt% **16:0**	LD	23.3 ± 0.4^{c}	11.2 ± 0.1^{c}		-41.4 ± 3.6^{bc}	16.0 ± 0.4^{b}	32.6 ± 0.4^{a}	35.6 ± 0.2^{a}	50.1 ± 8.1^{a}	21.0 ± 0.5^{a}	41.0 ± 0.4^{b}	59.6 ± 11.5^{a}
	MD	21.6 ± 0.6^{c}	19.2 ± 0.5^{d}	9.0 ± 0.6^{a}	-36.0 ± 3.2^{bc}	17.2 ± 0.3^{c}	33.4 ± 1.9^{a}	35.2 ± 0.5^{a}	45.7 ± 7.7^{a}	21.5 ± 0.2^{a}	49.0 ± 0.1^{c}	59.8 ± 3.2^{a}
	SD	21.3 ± 1.0^{c}	16.3 ± 0.4^{d}	4.6 ± 0.1^{c}	-23.8 ± 4.3^{ab}	13.0 ± 0.3^{a}	30.6 ± 0.1^{a}	35.4 ± 0.5^{a}	48.4 ± 9.8^{a}	21.8 ± 0.2^{a}	36.0 ± 0.5^{a}	42.5 ± 7.2^{a}
AMF+ 5 wt% **PPP**	LD	21.3 ± 0.4^{d}	14.0 ± 0.1^{b}	8.1 ± 0.1^{a}	-42.9 ± 2.2^{c}	16.0 ± 0.4^{b}	38.8 ± 0.4^{b}	41.8 ± 0.3^{b}	54.2 ± 8.8^{a}	21.2 ± 0.5^{a}	46.0 ± 0.4^{c}	71.1 ± 13.7^{a}
	MD	18.4 ± 0.2^{b}	13.5 ± 0.1^{c}	7.7 ± 0.1^{b}	-38.4 ± 1.2^{c}	16.8 ± 0.3^{c}	39.2 ± 2.3^{b}	45.6 ± 0.6^{b}	49.2 ± 8.3^{a}	21.4 ± 0.2^{ab}	46.0 ± 0.1^{b}	63.7 ± 3.4^{a}
	SD	15.1 ± 0.6^{b}	9.7 ± 0.4^{c}		-36.2 ± 1.8^{c}	17.4 ± 0.4^{b}	33.2 ± 0.1^{b}	45.6 ± 0.6^{b}	43.3 ± 8.8^{a}	21.6 ± 0.2^{a}	45.5 ± 0.6^{b}	49.8 ± 8.4^{a}

[1] T_{onset}: initial crystallization temperature upon cooling; T_{offset}: upper melting temperature.
[2] When thermograms present several endothermic or exothermic events, T_{peak} is taken at the maximum of each peak. Only the position of the most intense peaks is reported.
[3] ΔH: melting or crystallization enthalpy variations, determined from the total area of the thermographs between 4 °C and T_{onset} or T_{offset}, the temperature at which the DSC signal leaves or reaches the baseline.

[4] Values are expressed as mean ± standard deviations. n = 3 independent repetitions for all crystallization experiments and for melting experiments with emulsions containing neat AMF. n=1 for melting experiments with emulsions containing modulators; for the statical analysis, the same relative standard deviations (SD/mean) as those of the emulsions based on neat AMF with comparable average droplet sizes were adopted. For a given droplet size, mean values with unlike superscript letters are significantly different ($p < 0.05$) using a one-way analysis of variance followed by a pairwise t-test. Within the neat AMF group, mean values with unlike symbols were significantly different ($p < 0.05$).

Figures

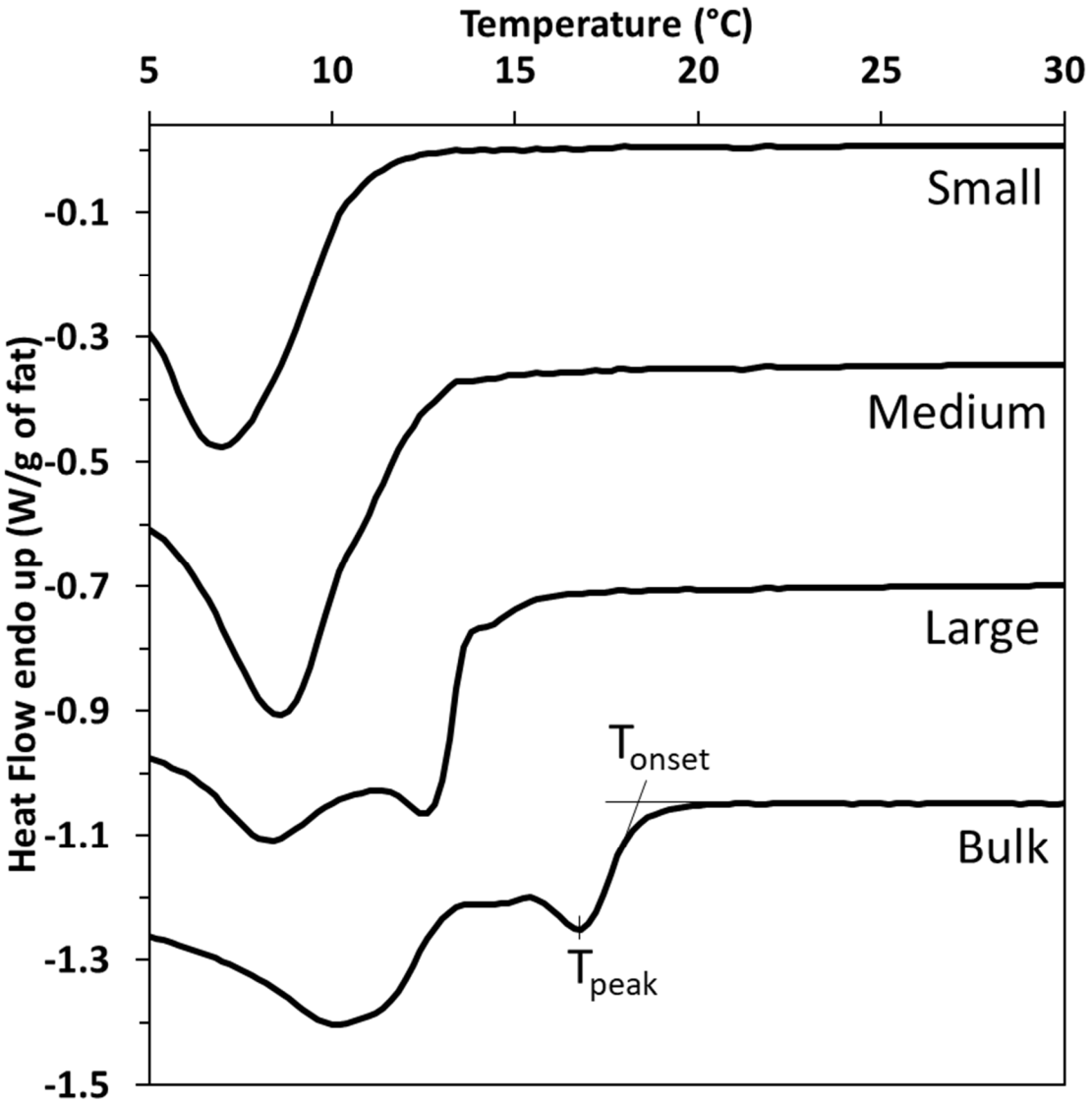

Figure 1

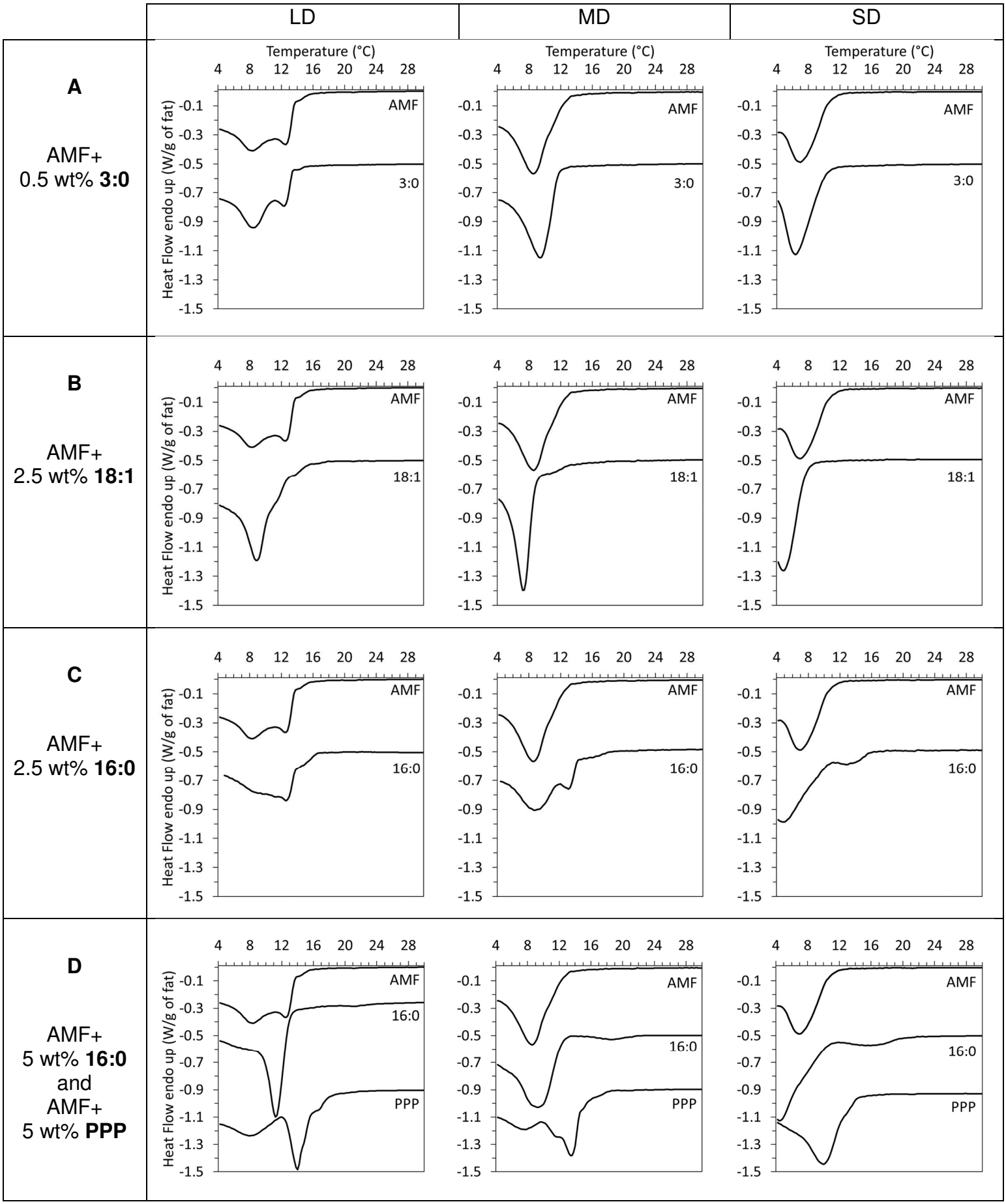
LD
MD
SD
A
AMF+
0.5 wt% 3:0
B
AMF+
2.5 wt% 18:1
C
AMF+
2.5 wt% 16:0
D
AMF+
5 wt% 16:0
and
AMF+
5 wt% PPP
Temperature (°C)
4 8 12 16 20 24 28
Heat Flow endo up (W/g of fat)
-0.1 -0.3 -0.5 -0.7 -0.9 -1.1 -1.3 -1.5
AMF
3:0
18:1
16:0
PPP

Figure 2

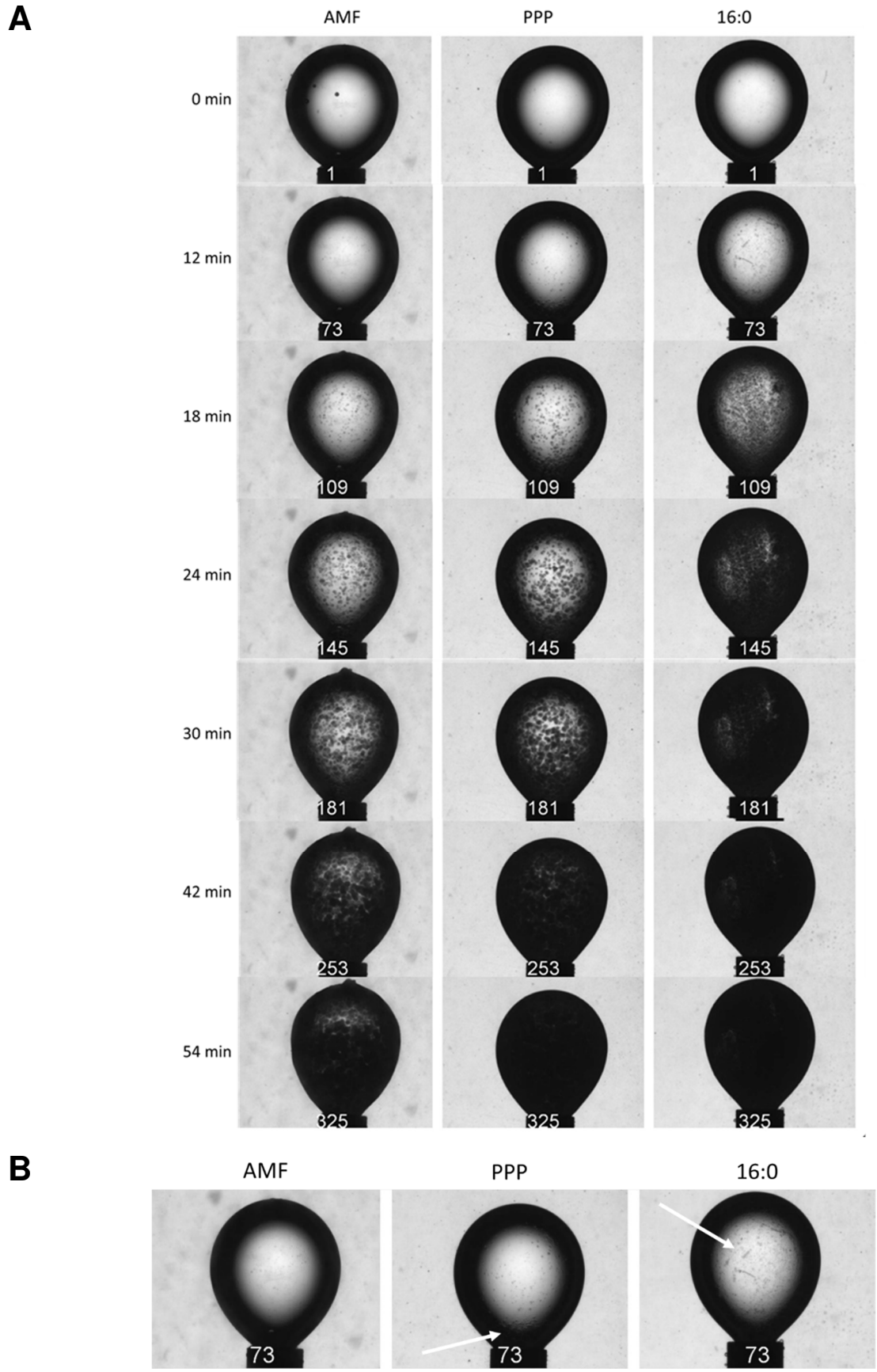
A
AMF
PPP
16:0
0 min
12 min
18 min
24 min
30 min
42 min
54 min
1
73
109
145
181
253
325
B
AMF
PPP
16:0
73
73
73

Figure 3

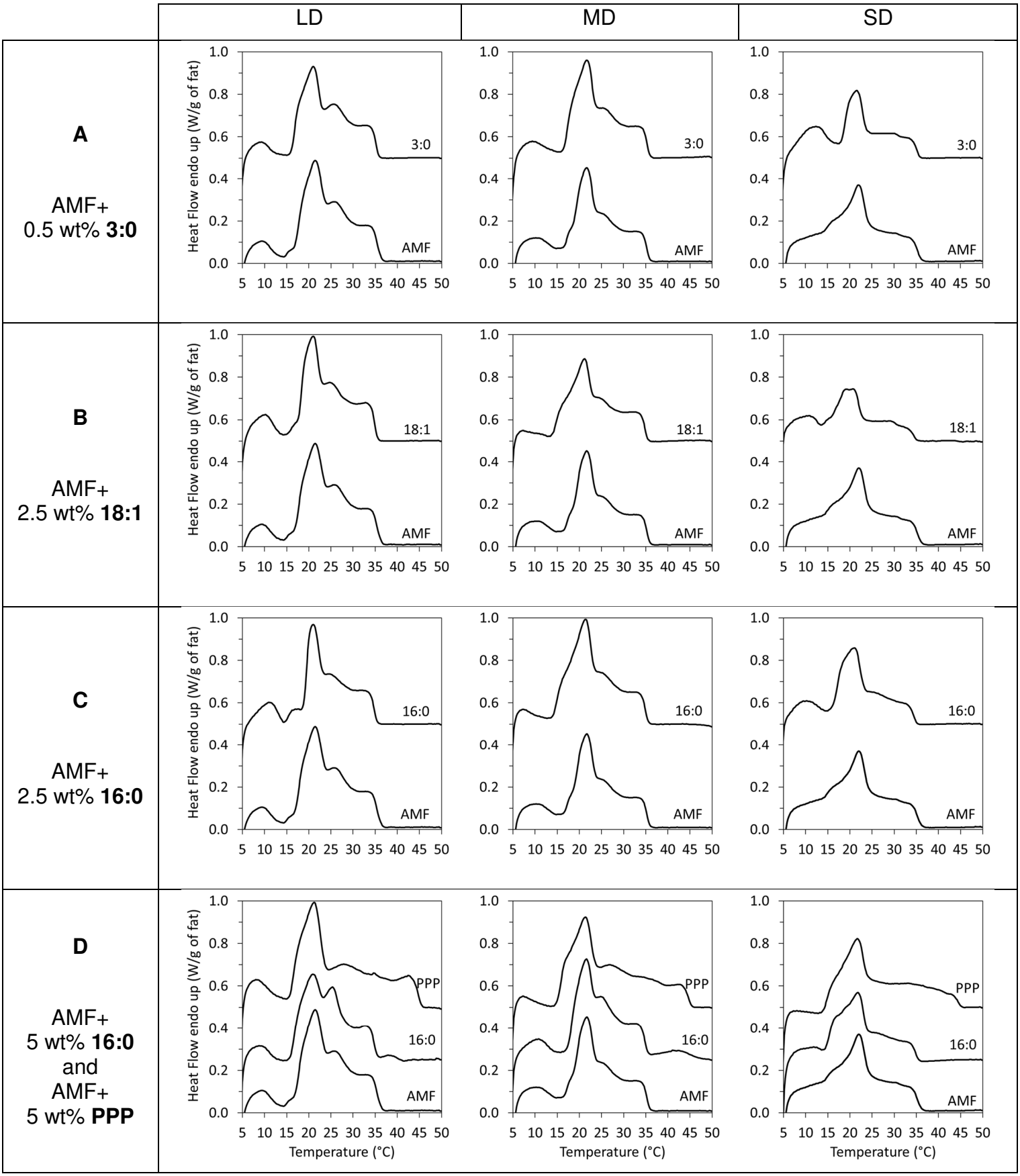
LD
MD
SD
A
AMF+
0.5 wt% 3:0
B
AMF+
2.5 wt% 18:1
C
AMF+
2.5 wt% 16:0
D
AMF+
5 wt% 16:0
and
AMF+
5 wt% PPP
Heat Flow endo up (W/g of fat)
Temperature (°C)
3:0
18:1
16:0
PPP
AMF

Figure 4